

MASS WASTING IN PLANETARY ENVIRONMENTS: IMPLICATIONS FOR SEISMICITY. R. C. Weber,¹ A. L. Nahm², and N. Schmerr³, ¹NASA Marshall Space Flight Center (renee.c.weber@nasa.gov), ²University of Idaho, ³University of Maryland.

Introduction: On Earth, mass wasting events such as rock falls and landslides are well known consequences of seismically generated ground motion. Through a variety of remote sensing techniques, tectonic faults have been positively identified on all four of the inner planets, Earth's Moon, several outer planet satellites, and asteroids [1]. High-resolution imaging has enabled positive identification of mass wasting events on many of these bodies. On Mars, it has been suggested that fallen boulders may be indicative of paleomarsquakes [2]. On the Moon, impacts and moonquakes have likewise been suggested as potential triggering mechanisms for mass wasting [3]. Indeed, we know from the Apollo era that the Moon experiences a wide variety of seismicity [4].

Seismicity estimates play an important role in creating regional geological characterizations, which are useful for understanding a planet's formation and evolution, and of key importance to site selection for landed missions. Here we investigate the regional effects of seismicity in planetary environments with the goal of determining whether surface features such as landslides and boulder trails on the Moon, Mars, and Mercury are triggered by fault motion (Fig. 1). We aim to quantify the amount of near-source ground shaking necessary to mobilize the material observed in various instances of mass wasting.

Lobate scarps: Lobate scarps, the typical surface expressions of thrust faults resulting from tectonic compression, are widely observed on the Moon, Mars, and Mercury (Fig. 2). Compared to other types of tectonic faults, surface-cutting thrust faults require the largest amount of stress to form and/or slip, and thus are expected to result in large quakes. While normal faults, graben, and wrinkle ridges may be more abundant on Mars, the Moon, and Mercury respectively, these structures would generate smaller theoretical maximum quakes than lobate scarp thrust faults. Thus, we optimize our chances of finding mass wasting associated with faults by studying lobate scarps.

Methodology: We first focus on calculating the theoretical maximum quake that could occur as a result of slip on a given fault and then determine the resulting effects on the surrounding surface morphology. The expected damage area indicated by seismic wavefield modeling is compared to mapped imagery to determine the likelihood of a quake having triggered a mass wasting event.

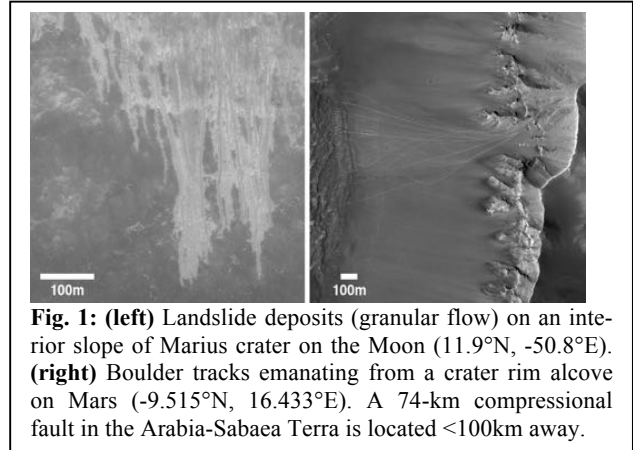


Fig. 1: (left) Landslide deposits (granular flow) on an interior slope of Marius crater on the Moon (11.9°N, -50.8°E). **(right)** Boulder tracks emanating from a crater rim alcove on Mars (-9.515°N, 16.433°E). A 74-km compressional fault in the Arabia-Sabaea Terra is located <100km away.

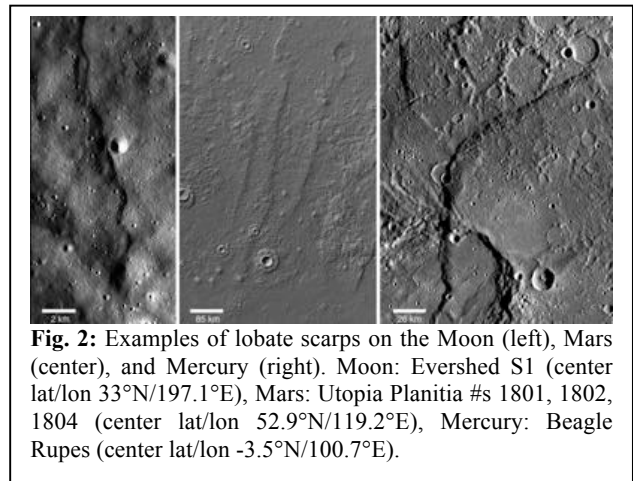


Fig. 2: Examples of lobate scarps on the Moon (left), Mars (center), and Mercury (right). Moon: Evershed S1 (center lat/lon 33°N/197.1°E), Mars: Utopia Planitia #s 1801, 1802, 1804 (center lat/lon 52.9°N/119.2°E), Mercury: Beagle Rupes (center lat/lon -3.5°N/100.7°E).

Theoretical maximum quake. Following the method outlined in [5], the theoretical maximum quake magnitude is derived from basic fault properties. These are either estimated from imagery or derived from laboratory rock experiments or elastic dislocation models, and include the length (L), fault dip angle (δ), depth of faulting (T), and fault width (w) (Fig. 3). Fault displacement (D) is calculated using displacement-length scaling such that $D = \gamma L$, where γ is determined by rock type and tectonic setting [6]. We note that subsurface fault geometry and mechanical properties of planetary lithospheres and regoliths are not completely understood, and thus represent potential sources of uncertainty in the maximum quake calculation. To incorporate this uncertainty, we investigate ranges in fault parameters, placing upper and lower bounds on

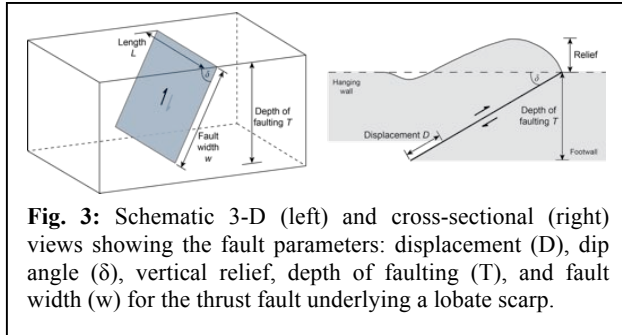


Fig. 3: Schematic 3-D (left) and cross-sectional (right) views showing the fault parameters: displacement (D), dip angle (δ), vertical relief, depth of faulting (T), and fault width (w) for the thrust fault underlying a lobate scarp.

our maximum quake calculations rather than estimating discrete values.

The best measure of the size of a planetquake is the seismic moment, M_0 . Seismic moment is calculated by multiplying the shear modulus of the ruptured rock (G) by the area of the ruptured portion of the fault (A) and the average displacement (D) produced during the quake, such that $M_0 = GAD = G(Lw)(\gamma L)$ [5]. The seismic moment represents the total energy consumed in producing displacement on a fault, regardless of the local strain rate or fault formation mechanism.

Seismic wavefield modeling. In order to determine the dimensions of an area affected by seismic shaking, we model the ground motion resulting from the theoretical maximum quake along a given fault (Fig. 4). Following the method of [7], we use the Serpentine Wave Propagation Program (WPP), a numerical code for simulating seismic wave propagation through arbitrary elastic and anelastic media in a 3D model space [8]. The initial model of a given fault includes regional 3D topography derived from digital elevation models, and the planet's relevant background 1D velocity.

We note that the modeled peak ground motion is less strongly dependent upon the choice of background velocity model than upon the scattering and attenuation properties of the shallowest materials in the model. Synthetic seismograms for the Moon most reasonably approximating those recorded by the Apollo seismometers are acquired for a 1 km thick, highly scattering layer as the topmost layer in the model. Similar highly fractured layers are expected on Mars and Mercury, and we approximate their velocities using the physical properties of a basaltic crust for each body.

Mass Wasting Modeling: Peak vertical ground velocity (a proxy for displacement) occurs within a few kilometers of the main shock and drops off rapidly away from the source. Thus we should expect most of the mass wasting phenomena to occur in the immediate vicinity of the fault. However, this result may depend on regional effects such as surface slope and megaregolith thickness; a thicker megaregolith (as might be expected in the vicinity of large craters) would tend to focus shaking in some of the crater ba-

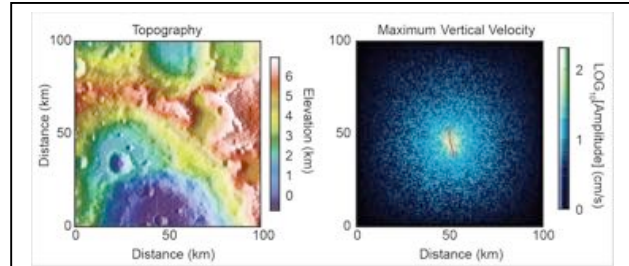


Fig. 4: Predicted ground motion in the vicinity of the Evershed lobate scarp on the Moon. **Left:** Surface topography input into the simulation, from the Lunar Orbiter Laser Altimeter experiment. The Evershed scarp is centered in the image (see Fig. 2). **Right:** Ground motion for a magnitude 7.8 quake on a subjacent reverse fault, with $T=2.25$ km. The surface trace of the scarp is indicated by the red line. A random distribution of heterogeneity of 25% in seismic wave velocity with 100 km scale length scatterers is placed in the lunar megaregolith to simulate the scattering typically present in lunar seismograms. Peak ground velocity is measured for the first 1000 seconds of the seismic trace.

sins. The presence of sediments also enhances seismic shaking; this could be relevant for Martian craters that may have been lakes some time in the past.

We will compare the observed extent of mass wasting in the vicinity of a fault to the modeled event magnitude and peak ground motion in order to establish a method to translate quake parameters into mass wasting estimates. This has been performed for terrestrial examples focused on determining landslide area and density over time in seismically active regions [9], as well as using the presence or absence of precariously perched boulders as indicators of the vigor of regional seismic shaking. The latter example has also been performed on Mars, where both boulder size and boulder trail density were found to peak close to the center of a fault system and decrease linearly along strike [2]. We expect to find systematic variations in fit parameter estimates for each body, reflecting different gravitational strengths, regolith cohesion properties, and other geologic settings local to each body/study region.

References: [1] Watters, T. R. and Schultz, R. A. (2010) *Cambridge University Press*. [2] Roberts, G. P. et al. (2012) *JGR*, 117, doi:10.1029/2011JE003816. [3] Xiao, Z. et al. (2013) *Earth Planet. Sci. Lett.* 376, 1–11. [4] Weber, R. C. (2014) Elsevier, 539–554. [5] Nahm, A. L. and Velasco, A. A. (2013) LPSC 44th, Abstract #1422. [6] Cowie, P. A. and Scholz, C. H. (1992) *J. Struct. Geol.* 14, 1149–1156. [7] Schmerr, N. et al. (2013) LPSC 44th, Abstract #2438. [8] Sjogreen, B. and Petersson, N. A. (2012) *J. Sci. Comp.* 52, 17–48. [9] Meunier, P. et al. (2007) *GRL* 23, doi:10.1029/2007GL031337.